THE JOURNAL OF PHYSICAL CHEMISTRY B

ARTICLE

pubs.acs.org/JPCB

Circularly Polarized Luminescence as a Probe for Long-Range Interactions in Molecular Aggregates

Roel Tempelaar,[†] Anna Stradomska,[†] Jasper Knoester,[†] and Frank C. Spano*[,‡]

[†]Zernike Institute for Advanced Materials, University of Groningen, Nijenborgh 4, 9747 AG Groningen, The Netherlands

[‡]Department of Chemistry, Temple University, Philadelphia, Pennsylvania 19122, United States

ABSTRACT: The extreme sensitivity of circularly polarized luminescence (CPL) to long-range excitonic interactions inside a helical aggregate is investigated. It is found to persist even in the presence of strong energetic disorder and coupling of the exciton to molecular vibrations, when the emitting exciton is localized to only a few chromophores. The CPL dissymmetry, g_{lum}, is found to depend on a modulated sum over the excitonic couplings, $\Sigma_{n,s} J_{n,n+s}\, s\, \sin(\phi s)$, where $J_{n,n+s}$ is the coupling between molecules separated by s lattice spacings and ϕ is the pitch angle between adjacent chromophores. The validity of this relation is confirmed through full-scale numerical simulations of helical MPOV4 aggregates using the disordered Holstein Hamiltonian. In addition, an analytical expression for g_{lum} is obtained for a helical chain containing a single, energetically detuned chromophore to represent strong disorder. Subsequently, the resulting expression is generalized to include full distributed disorder. Our results demonstrate that the spatial dependence of extended interactions can be extracted from experimental spectra, without having details on disorder or exciton-vibrational coupling.

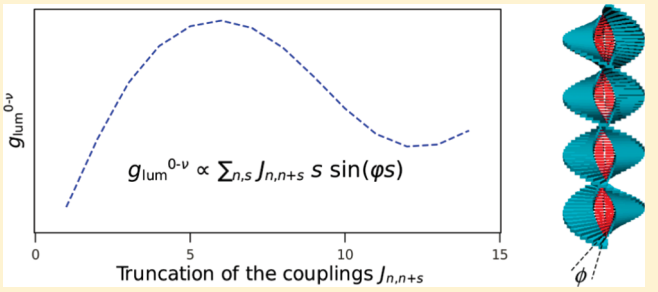

1. INTRODUCTION

In addition to unpolarized absorption and luminescence, circular dichroism (CD) and circularly polarized luminescence (CPL) spectroscopies are powerful tools for probing the electronic structure of chiral molecular systems.[1,2] Such techniques are especially useful for studying excited states in chiral self-assembled supramolecular aggregates which utilize hydrogen bonding and/or $\pi-\pi$ stacking interactions, involving a variety of chromophores.[3−11] Over the past several years, interest in these systems has blossomed, driven in large part by the promise of more efficient organic electronic devices.

Almost 40 years ago, Harada[12] recognized the high sensitivity of the CD response to long-range intermolecular couplings, inspiring a number of studies by others exploring the CD signal from two distant chromophores.[13−15] Harada showed that in a dimer, the bisignate CD response scales as $\mathbf{R}_{1,2}\cdot(\boldsymbol{\mu}_1 \times \boldsymbol{\mu}_2)J_{1,2}$, where $\mathbf{R}_{1,2}$ is the vector separation between chromophores 1 and 2 with respective transition dipole moments $\boldsymbol{\mu}_1$ and $\boldsymbol{\mu}_2$, and where $J_{1,2}$ is the intermolecular interaction. Hence, the effect of distant chromophores on the CD signal is of a much longer range ($\sim 1/{R_{1,2}}^2$) than the coupling, which scales as $J_{1,2} \sim 1/{R_{1,2}}^3$. More recent studies on chiral aggregates confirmed the sensitivity to long-range electronic couplings and showed that the first moment of the CD spectrum is entirely independent of the amount of static (inhomogeneous) broadening[16−18] and even the coupling to molecular vibrations.[18] Remarkably, the sensitivity of CD remains practically unchanged in the presence of strong disorder, where the exciton is localized over only one or two chromophores.[18] This makes CD spectroscopy far superior to unpolarized absorption measurements for detecting distant intermolecular interactions in molecular assemblies.

The CPL dissymmetry, $g_{\mathrm{lum}}(\omega)$, has also been utilized as a probe of excited state properties in organic molecules and assemblies.[19−24] In contrast to CD spectroscopy, which generally provides information about the most strongly allowed states, CPL directly probes only the low-energy emitting states. The dissymmetry is defined as the difference between left- and right-handed circularly polarized luminescence normalized to the total emission intensity, that is

$$g_{\mathrm{lum}}(\omega) \equiv 2\,\frac{S_{\mathrm{L}}(\omega) - S_{\mathrm{R}}(\omega)}{S_{\mathrm{L}}(\omega) + S_{\mathrm{R}}(\omega)} \qquad (1)$$

where $S_{\mathrm{L(R)}}(\omega)$ is the frequency-dependent emission intensity of the left (right) circularly polarized component. It has been shown that $g_{\mathrm{lum}}(\omega)$ contains a wealth of information about the emitting state, which is best described as an excitonic polaron composed of a vibronically excited "center" with vibrationally excited neighbors. In particular, careful analysis of $g_{\mathrm{lum}}(\omega)$ yields the exciton coherence length as well as the polaron radius.[25−27]

The helical assemblies attracting the greatest attention so far are those composed of monofunctionalized oligo-phenylene-vinylene (MOPV4) chromophores,[3−5,28−34] where 4 is the number of phenyl groups in the OPV. At low temperatures, MOPV4 chromophores in solution self-assemble into a helical

Received: June 6, 2011
Revised: July 26, 2011
Published: August 18, 2011

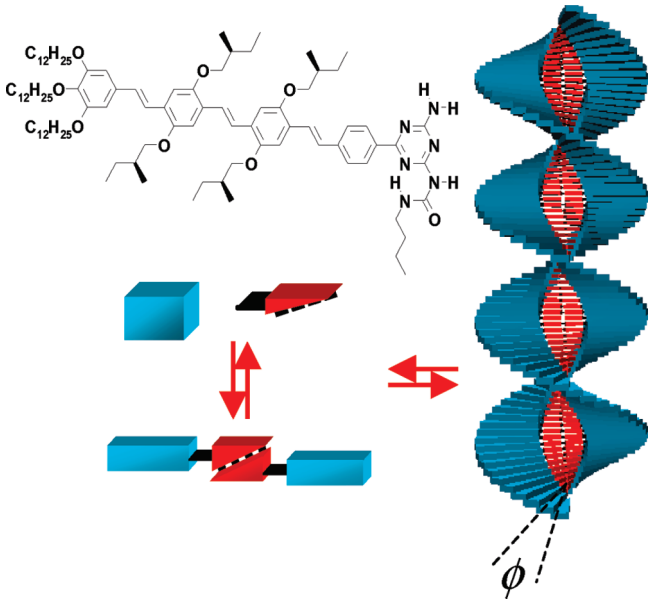

Figure 1. Schematic representation of the self-assembly of a helical MOPV4 aggregate. The OPV4 backbone (blue block) is capped with a functional H-bonding end group (red block). Two H-bonded functionalized chromophores form a rung of the helical supramolecular structure. The distance between two consecutive rungs is d = 3.75 Å, and their relative pitch angle is ϕ = 14°. Also demonstrated is the molecular structure of the OPV4 chromophore.

supramolecular structure, where each rung of the helix consists of two MOPV4 units hydrogen-bonded through the triazine head groups, see Figure 1. Aggregation is manifested by the emergence of a bisignate CD signal encompassing the lowest molecular singlet transition, as well as the appearance of a low-energy shoulder in the corresponding absorption spectrum.[28] Additional signatures of aggregation include a red-shift of the photoluminescence (PL) spectrum along with the appearance of a nonzero $g_{\mathrm{lum}}(\omega)$ signal.[28] The PL spectrum features a clear vibronic progression due to linear coupling of the emitting exciton to an intramolecular symmetric ring breathing/vinyl stretching vibrational mode with an energy of 172 meV (1400 cm^{-1}). The corresponding $|g_{\mathrm{lum}}(\omega)|$ decreases monotonically from its peak value near the 0 − 0 transition toward the lower-energy sidebands. All of these features have been well-accounted for via exciton theory.[25]

In a prior MOPV4 study, the emitting exciton's spatial coherence length was derived from $g_{\mathrm{lum}}(\omega)$. The analysis, which yielded a coherence length of only a few angstroms due to strong disorder-induced localization, was based on the unique sensitivity of the 0−0 transition to exciton coherence.[26] By contrast, the dissymmetry in the vicinity of the sidebands (0−1, 0−2, ...) is not coherently enhanced, but its magnitude does provide information about the radius of the excitonic polaron, which is also quite small.[25] In the special case of a disorder-free helical aggregate, where the exciton wave function is delocalized over the entire aggregate, the sideband $g_{\mathrm{lum}}(\omega)$ was also shown to be highly sensitive to long-range interactions, similar to the CD response.[26] Numerical calculations in ref 25 further showed that for disordered MOPV4 helices, despite the small coherence length, the CPL dissymmetry remains sensitive to extended interactions: truncating the electronic couplings beyond 6 nearest neighbors resulted in an astounding 30% increase in $g_{\mathrm{lum}}(\omega)$, despite a practically indiscernible change in the unpolarized PL spectrum.

The purpose of this work is to further investigate the sensitivity of $g_{\mathrm{lum}}(\omega)$ to extended interactions in helical molecular aggregates. Our primary goal is to understand how such sensitivity can survive the localizing effects of disorder. Both exciton-vibrational coupling and disorder are taken into account using the model originally introduced in ref 25. This model has proven successful in reproducing the unpolarized absorption and luminescence spectral line shapes of MOPV4 helices, as well as their CD and CPL dissymmetry spectra. The model highlights the profound importance of the vibronic/vibrational pair states, also called two-particle states, in $g_{\mathrm{lum}}(\omega)$. Were it not for such states, the sideband contributions to $g_{\mathrm{lum}}(\omega)$ would be exactly zero. Further details on the model are given in section 2, together with numerical results for MOPV4, obtained using an uncorrelated Gaussian distribution of chromophoric transition energy offsets. An analytical expression for $g_{\mathrm{lum}}(\omega)$ is presented in section 3 for the single impurity scattering (SIS) model. The SIS model mimics the effects of disorder by introducing a single chromophore energetically detuned by $-\Delta$ in an otherwise homogeneous aggregate. The model is solved using perturbation theory to the lowest orders in W/Δ, where W is the free exciton bandwidth. In section 4, we return to the Gaussian disorder model and obtain a perturbative expression for $g_{\mathrm{lum}}(\omega)$ to first order in W/ω_0. The advantage here is that we can treat the limit of weak disorder, which was inaccessible with the SIS model. For both models $g_{\mathrm{lum}}(\omega)$ reveals the dependence on extended couplings, thereby affirming its ability to sense long-range interactions.

2. MODEL AND NUMERICAL RESULTS

In this section a full numerical study is presented on the sensitivity of CPL dissymmetry to extended excitonic interactions, with an emphasis on the impact of disorder. In doing so, helical MOPV4 aggregates are used as a model system, which is described by the disordered Holstein Hamiltonian. Upon numerical diagonalization of the Hamiltonian, the PL and CPL dissymmetry spectra are calculated for different truncation distances of the interactions. Both the disorder-free and strongly disordered cases are taken into account. Our numerical results suggest a simple scaling relationship between $g_{\mathrm{lum}}(\omega)$ and the excitonic couplings, whose general form is independent of disorder and exciton-vibrational coupling. A further analytical investigation of this equation is presented in sections 3 and 4.

The numerical calculations of MOPV4 are based on the model as introduced in ref 25. Following an effective single-strand approximation,[25] the aggregate is considered as a linear chain consisting of N two-level chromophores with radially oriented transition dipoles. The average chromophore $S_0 \rightarrow S_1$ transition energy is $\omega_{0-0} + D$, where ω_{0-0} is the gas-phase 0−0 frequency and D is the gas-to-crystal shift. Throughout the calculations, this average transition energy is taken as $\omega_{0-0} + D$ = 2.53 eV. Disorder is taken into account by including an energy offset Δ_n for each chromophore n. These energetic fluctuations along the aggregate are caused by thermally induced deformations within each chromophore (e.g., by twisting and bending), fluctuations of the conformations of the chromophoric side groups, or randomness in the environment because of the presence of solvent molecules. The effect of disorder is simulated by drawing the energy offsets randomly from a normal distribution with a standard deviation σ, that is $P(\Delta_n) = [\sigma(2\pi)^{1/2}]^{-1} \exp(-\Delta_n^2/2\sigma^2)$.

dx.doi.org/10.1021/jp2053019 |J. Phys. Chem. B 2011, 115, 10592–10603

The excitonic interactions between the chromophores in an MOPV4 aggregate are taken from ref 25. These couplings have been evaluated by combining a coupled cluster singles and doubles (CCSD) approach with the INDO Hamiltonian on the basis of geometric structures as obtained from MD calculations.[31] The corresponding free exciton bandwidth, that is, the energy difference between the highest- and lowest-energy exciton in a disorder-free aggregate without vibronic coupling, is $W = 150$ meV.

The $S_0 \rightarrow S_1$ electronic excitation within each chromophore couples linearly to the intramolecular symmetric ring breathing/vinyl stretching mode with a vibrational energy of $\omega_0 = 172$ meV, leading to a polaronic exciton. The corresponding shift in the nuclear potential upon electronic excitation is characterized by a Huang−Rhys factor of $\lambda^2 = 1.2$.[35]

The MOPV4 helix described above is modeled by the disordered Holstein Hamiltonian,[36] which includes all of the aforementioned contributions. In the one-exciton representation it reads

$$H = \omega_0 \sum_n b_n^\dagger b_n + \lambda\omega_0 \sum_n (b_n + b_n^\dagger)|n\rangle\langle n| + \lambda^2\omega_0 + \sum_{m,n} (J_{m,n} + \Delta_m \delta_{m,n})|m\rangle\langle n| + \omega_{0-0} + D \quad (2)$$

where $\hbar = 1$ is taken. The vibrational energy is described by the first term, where $b_n^\dagger$ (b_n) creates (annihilates) a vibrational quantum at chromophore n within the electronic ground state nuclear potential. The second and third terms represent the exciton-vibrational coupling. $|n\rangle$ indicates the pure-electronic state in which chromophore n is electronically excited to S_1, whereas all other chromophores reside in the electronic ground state S_0. The fourth term contains the excitonic coupling between chromophores m and n, denoted as $J_{m,n}$. This term also includes the chromophore-dependent site disorder Δ_n.

For MOPV4, the (free) exciton bandwidth, the vibrational energy ω_0 and the vibronic relaxation energy $\lambda^2\omega_0$ are all comparable in magnitude, corresponding to the intermediate coupling regime. In this regime, the eigenstates of the disordered Holstein Hamiltonian are described highly accurately[37] by using the two-particle approximation.[37,38] Accordingly, the αth eigenstate is expanded as

$$|\Psi^{(\alpha)}\rangle = \sum_{n,\tilde{\nu}} c_{n,\tilde{\nu}}^{(\alpha)} |n,\tilde{\nu}\rangle + \sum_{n,\tilde{\nu}} \sum_{n',\nu'} c_{n,\tilde{\nu};n',\nu'}^{(\alpha)} |n,\tilde{\nu};n',\nu'\rangle \quad (3)$$

The one-particle state $|n,\tilde{\nu}\rangle$ is a vibronic (both electronically and vibrationally excited) state at chromophore n, containing $\tilde{\nu}$ vibrational quanta in the shifted potential of the electronic excited state. This term describes the polaron's center of mass. $|n,\tilde{\nu};n',\nu'\rangle$ denotes a two-particle state, in which a vibronic excitation at chromophore n is accompanied by $\nu' \geq 1$ vibrational quanta in the ground-state potential of molecule n'. This two-particle term is responsible for the polaron radius. (Note that $\tilde{\nu}$ including the tilde corresponds to vibrational quanta in the shifted potential, whereas ν corresponds to quanta in the unshifted potential.) The two-particle approximation greatly reduces the size of the basis set. Additionally, in both the one-particle and two-particle states, the total number of vibrational quanta ($\tilde{\nu}+\nu'$) is limited to ν_{max}. In all calculations to follow, $\nu_{max} = 4$ is taken, unless otherwise stated. This value is sufficiently high to ensure convergent spectra.

After calculating the eigenstates of the Hamiltonian in the two-particle representation, the reduced[39] PL spectrum and CPL dissymmetry spectrum are evaluated. The former is represented by the expression

$$S(\omega) = \sum_{\nu_t = 0,1,\ldots} \langle I^{0-\nu_t}(C)\Gamma(\omega - \omega_{em(C)} + \nu_t\omega_0)\rangle_C \quad (4)$$

where $\langle ... \rangle_C$ denotes an average over random configurations (C) of site transition energies. The line shape function $\Gamma(\omega - \omega_{em(C)} + \nu_t\omega_0)$ is taken to be a Gaussian, centered at the $0-\nu_t$ transition energy $\omega_{em(C)} - \nu_t\omega_0$, with its standard deviation σ_H representing the homogeneous line width. This line width is set to $\sigma_H = 14$ meV throughout this paper. The emission is assumed to occur after the thermal equilibrium is reached within the manifold of excited states; furthermore, k_BT is assumed low enough, so that emission only takes place from the lowest-energy eigenstate, denoted by $|\Psi^{(em)}\rangle$ with corresponding eigenenergy ω_{em}. Both are dependent on the randomly generated configuration of transition energies (C). Upon emitting radiation, the aggregate makes a transition to the electronic ground state, which may be vibrationally excited, with a total of ν_t vibrational quanta. This $0-\nu_t$ transition is characterized by a configuration-dependent line strength, given by

$$I^{0-\nu_t}(C) = \frac{1}{\mu^2} \sum_{\{\nu_n\}}{}' |\langle \Psi^{(em)}(C)|\hat{\mathbf{M}}|G\{\nu_n\}\rangle|^2 \quad (5)$$

Here, the summation over $\{\nu_n\}$ extends over all possible vibrational configurations in the (final) ground state $|G\{\nu_n\}\rangle \equiv |g_1,\nu_1; g_2,\nu_2;\ldots;g_N,\nu_N\rangle$, with the restriction that the sum of all vibrational quanta equals ν_t, as indicated by the prime. The aggregate transition dipole moment $\hat{\mathbf{M}}$ consists of a sum of the transition dipole moment vector operators of the individual chromophores

$$\hat{\mathbf{M}} = \sum_n |n\rangle\langle g|\boldsymbol{\mu}_n + \text{h.c.} \quad (6)$$

With the $\mathbf{k}$ direction defined along the helix axis, the radially directed transition dipole moment vector reads $\boldsymbol{\mu}_n = \mu[\cos(\phi n)\mathbf{i} - \sin(\phi n)\mathbf{j}]$. The pitch angle is set to $\phi = 14°$, as appropriate for MOPV4,[25] a value which corresponds to a left-handed helix.

The expression for the spectrum of CPL dissymmetry reads[26]

$$g_{lum}(\omega) = \frac{4}{S(\omega)} \sum_{\nu_t = 0,1,\ldots} \langle R_{lum}^{0-\nu_t}(C)\Gamma(\omega - \omega_{em(C)} + \nu_t\omega_0)\rangle_C \quad (7)$$

which, in accordance with the Rosenfeld equation,[1] includes the rotational strength

$$R_{lum}^{0-\nu_t}(C) = \frac{i}{c\mu^2} \sum_{\{\nu_n\}}{}' \langle \Psi^{(em)}(C)|\hat{\mathbf{M}}|G\{\nu_n\}\rangle \cdot \langle G\{\nu_n\}|\hat{\mathbf{m}}|\Psi^{(em)}(C)\rangle \quad (8)$$

$\hat{\mathbf{m}}$ is the magnetic dipole operator, given by

$$\hat{\mathbf{m}} = \frac{ick}{2} \sum_n |n\rangle\langle g|\mathbf{r}_n \times \boldsymbol{\mu}_n + \text{h.c.} \quad (9)$$

with c denoting the speed of light and with k defined as $k = \omega_{FC}/c$. ω_{FC} is the single-molecule vertical (Franck−Condon) transition energy, taken here to be 2.85 eV. The individual chromophores are characterized by the position vector $\mathbf{r}_n = dn\mathbf{k}$, which points along the helix axis. The separation d between adjacent chromophores is set to 3.75 Å.[40] Finally, we note that the factor of 4 appearing in $g_{lum}(\omega)$ in eq 7 was absorbed in the definition of the

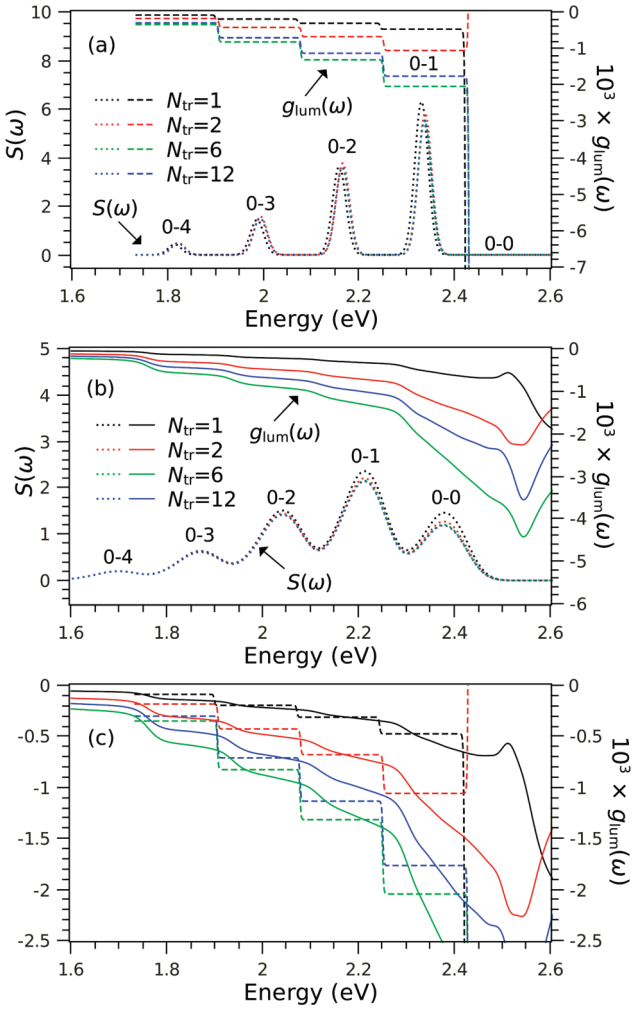

Figure 2. Calculated reduced PL (dotted lines) and CPL dissymmetry (solid/dashed lines) spectra at $T = 0$, for a helical aggregate containing $N = 15$ chromophoric units with a pitch angle of $\phi = 14°$. The calculated excitonic interactions from ref 25 are used, leading to a bandwidth of $W = 150$ meV for a disorder-free aggregate. The average chromophore transition energy is $\omega_{0-0} + D = 2.53$ eV. Exciton-vibrational coupling is included using a Huang−Rhys factor of $\lambda^2 = 1.2$ and a vibrational energy of $\omega_0 = 172$ meV. The homogeneous line width is $\sigma_H = 14$ meV. Shown are the results in the homogeneous limit (a) and for a disorder of $\sigma = 85$ meV (b), with a truncation of the interactions beyond $N_{tr} = 12$ (blue), 6 (green), 2 (red), and 1 (black) nearest neighbors. The CPL dissymmetry sideband spectra for both the disorder-free and the disordered case are shown in (c).

rotational strength in ref 26, thereby having no effect on $g_{lum}(\omega)$. A similar factor of 4 arises in the absorption dissymmetry and has been discussed at length in ref [16].

The resulting PL and CPL dissymmetry spectra are shown in Figure 2, for an MOPV4 aggregate consisting of $N = 15$ chromophores. Panel a shows the results in the disorder-free case, or homogeneous limit, in which all chromophoric transition energies are equal. Panel b corresponds to strongly disordered aggregates with $\sigma = 85$ meV, the value which correctly reproduces the absorption signal spectral line width in MOPV4 helices.[25,41] In our calculations an average is taken over a total of 10^5 configurations of disorder. In Figure 2, the black lines correspond to aggregates in which the excitonic couplings are limited to nearest neighbors by setting the truncation radius $N_{tr} = 1$. Also shown are the results for $N_{tr} = 2$ (red lines), 6 (green lines), and 12 (blue lines). In the homogeneous limit, the emission frequency ω_{em} is unique, leading to well-resolved peaks in both the unnormalized CPL and PL spectra and, ultimately, to the staircase-like structure observed in $g_{lum}(\omega)$. This structure broadens considerably with disorder, where ω_{em} varies over the individual disorder configurations and peaks of different ν_t start to overlap. In Figure 2a, the 0−0 PL peak has negligible oscillator strength, due to the helical conformation being an almost perfect H-aggregate. Setting the pitch angle ϕ to zero would make the 0−0 transition strictly symmetry-forbidden.[42] The symmetry is broken by disorder, which explains the substantial 0−0 line strength present in the PL spectra of the disordered aggregates.

There is also a significant change in the 0−0 region of the g_{lum} spectrum in going from the homogeneous to the disordered limit. In the former, $g_{lum}(\omega)$ achieves very large magnitudes due to the nearly vanishing value of I^{0-0} in the denominator of eq 7, and even changes sign at $N_{tr} = 2$. The unique behavior of $g_{lum}(\omega)$ in the 0 − 0 spectral region has been studied in detail in refs 26, 27.[43] As opposed to the sideband spectral region, the 0−0 CPL dissymmetry relates to the exciton coherence length, which equals N for an aggregate without disorder. However, introduction of disorder localizes the coherence function and increases the 0−0 PL intensity. At the point where the exciton coherence is limited to only a few chromophoric units, the 0−0 $g_{lum}(\omega)$ is found to behave similar to the sideband replicas.

Figure 2a demonstrates that in the homogeneous limit the CPL dissymmetry is highly sensitive to the truncation of the excitonic interactions. Consider for example the spectrum in the 0−1 region. Extending the interactions beyond nearest neighbors ($N_{tr} = 1$) results in a very substantial increase in $|g_{lum}(\omega)|$. When 6 nearest neighbors are included ($N_{tr} = 6$), the magnitude of $g_{lum}(\omega)$ swells to roughly four times the value for $N_{tr} = 1$, but backs off by approximately 15% upon extending the truncation distance to $N_{tr} = 12$. In marked contrast, the PL spectrum is hardly changed, showing a small blue-shift when the interaction range is extended beyond nearest neighbors, with a corresponding slight decrease in the 0 − ν_t peak intensities. In fact, the largest change in the PL spectrum occurs in going from $N_{tr} = 1$ to $N_{tr} = 2$, with practically no change in the range $N_{tr} = 2$ to 12. Moreover, since the PL intensity is an extrinsic quantity, dependent on parameters such as the optical density, these small changes are difficult to measure. On the other hand, the intrinsic nature of $g_{lum}(\omega)$ makes its sensitivity to extended interactions far easier to confirm experimentally.

The CPL dissymmetry in helical aggregates arises from the chirality of the emitting exciton, which stems from its delocalization over the helix.[1,25,44] Therefore, the sensitivity of $g_{lum}(\omega)$ to extended interactions in homogeneous aggregates is not surprising. What is surprising, however, is that the sensitivity is practically unchanged in strongly disordered aggregates, where the excitation is substantially localized. In the MOPV4 aggregates of Figure 2b, the exciton coherence ranges over only about two molecules as demonstrated in refs 18 and 26, yet $g_{lum}(\omega)$ follows the same trend as in the homogeneous limit with very similar enhancements for increasing N_{tr}. Apparently, $g_{lum}(\omega)$ is sensitive to extended interactions over distances much greater than the coherence length. The associated PL spectral changes are smaller than in the homogeneous limit, with the blue-shift obscured by inhomogeneous broadening.

The dependence of $g_{lum}(\omega)$ on extended interactions is to some extent comparable to the case of circular dichroism (CD).

In earlier studies, it was shown that the CD response is very sensitive to long-range interactions.[12−18,45,46] In the simplest case of a dimer system, the difference between the maximum and the minimum of the bisignate CD signal was found to obey the equation $|CD_{max} - CD_{min}| \propto J_{1,2}d \sin\phi$.[12] A similar scaling to $J_{1,2}d \sin\phi$ was found for the sideband CPL dissymmetry line strengths in case of disorder-free dimers,[27] be it only in the limit of weak excitonic coupling ($W \ll \lambda^2\omega_0$). On the other hand, g_{lum}^{0-0} is not dependent on the interactions strength, but instead demonstrates unique behavior due to the coherent nature of the 0−0 transition.[26]

In site-disordered aggregates Somsen et al.[16] and Burin et al.[17] showed that the first moment of the bisignate CD spectrum rigorously scales as a sum over excitonic interactions $J_{n,n+s}$, modulated by $s \sin(\phi s)$, that is $M_{CD}^1 \propto \Sigma_{n,s} J_{n,n+s} s \sin(\phi s)$. The scaling of the first moment with the modulated interaction sum was subsequently shown by Van Dijk and co-workers[18] to hold in the simultaneous presence of disorder and exciton-vibrational coupling. Their result is independent of the exciton bandwidth, the amount and spatial correlation of disorder, and the strength of the exciton-vibrational coupling.[18]

In what follows, we will show that the same s-sine-modulated sum explains the sensitivity to extended interactions observed for $g_{lum}(\omega)$. As it turns out, the CPL dissymmetry line strengths in the sideband region ($\nu_t \geq 1$) are approximately proportional to this modulated sum, that is

$$g_{lum}^{0-\nu_t} \propto \sum_{n,s} J_{n,n+s} s \sin(\phi s) \qquad (10)$$

As already mentioned, this relationship holds equally for the 0−0 line strength, provided that disorder forces a localization of the excited state to only a few chromophores.

Unfortunately, simple expressions for the first moment of $g_{lum}(\omega)$, in analogy to CD, cannot be easily derived. The CD spectrum receives contributions from the complete set of electronically excited states (final states in the absorption process), which gives rise to the characteristic bisignate CD signal (Cotton effect). On the other hand, low-temperature $g_{lum}(\omega)$ is completely determined by the lowest-energy excited state (initial state in PL). Moreover, whereas the CD spectrum (as well as the 0−0 CPL dissymmetry) is a one-particle construct, where two-particle coefficients contribute only indirectly through normalization of the wave function, the sideband CPL dissymmetry is directly proportional to the two-particle coefficients in the emitting exciton,[27] thereby establishing $g_{lum}(\omega)$ as a direct measure of the polaron radius.[25] Consequently, the analysis of $g_{lum}(\omega)$ is considerably more complex than CD(ω), although approximate methods still allow for an analytic evaluation. This has been done for the homogeneous limit in ref 26, where eq 10 is obtained by applying perturbation theory to first order in W/ω_0. Similar perturbative methods can be utilized to obtain equivalent expressions for the inclusion of a single impurity into the electronic transition energies, and even for full distributed disorder, as will follow in sections 3 and 4 respectively.

Figure 3 demonstrates the calculated sideband CPL dissymmetry line strengths divided by $\Sigma_{n,s} J_{n,n+s} s \sin(\phi s)$, as a function of the truncation N_{tr} of the excitonic interactions, for the same parameters as used in Figure 2. These so-called "net g_{lum} line strengths" show approximate constant behavior, being flat throughout the entire N_{tr} interval, indicating that indeed the CPL dissymmetry line strengths scale with the modulated sum. Interestingly, the disordered case (solid lines) shows flatter

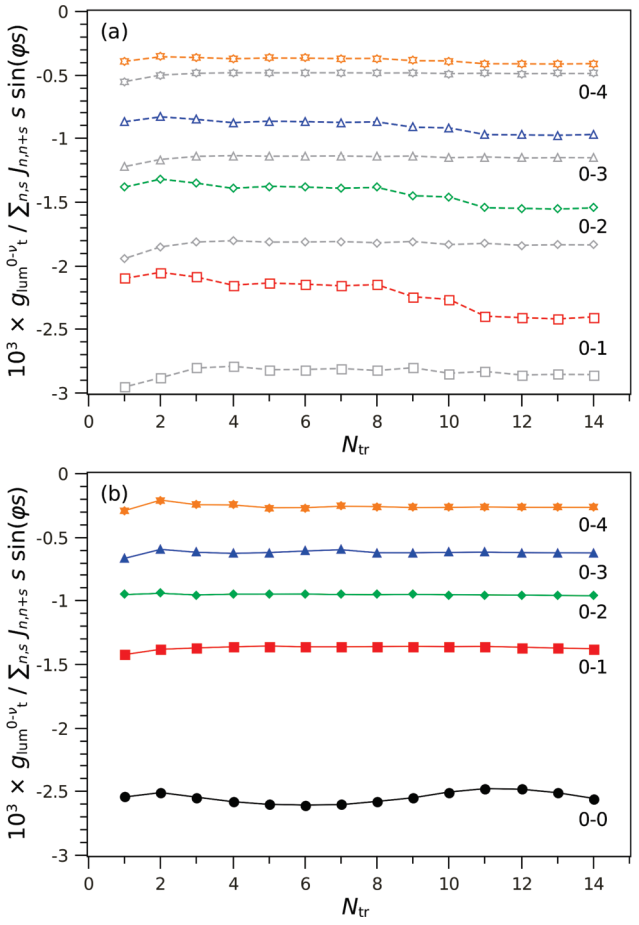

Figure 3. Calculated CPL dissymmetry line strengths divided by the $s \sin(\phi s)$-modulated sum over excitonic couplings, as a function of the truncation of the couplings. Shown are the results for $\nu_t = 0$ (black circles), 1 (red squares), 2 (green diamonds), 3 (blue triangles), and 4 (orange stars). Part (a) demonstrates the homogeneous limit, while the disordered case with $\sigma = 85$ meV is plotted in part (b). Also included in part (a) are the results for the homogeneous limit with the inclusion of pure-excitonic wave function coefficients in the modulated sum (gray symbols). The same parameters are used as in Figure 2.

results than the homogeneous case (dashed lines), demonstrating small deviations only for the 0−0 line strength and, in general, for $N_{tr} = 1$ and 2. In the homogeneous limit, the sideband curves show a characteristic fluctuation, best observed for 0−1. This fluctuation is due to the pure-excitonic wave function coefficients $\phi_{\bar{k},n}$ in the zeroth-order emitting state $|\bar{k},\tilde{\nu} = 0\rangle^0$, which appear inside the modulated sum as observed earlier in eq 29 of ref 26. Figure 3a demonstrates that inclusion of these coefficients in the modulated sum results in a further flattening-out of the net g_{lum} line strengths (gray curves). The extreme behavior of the 0−0 line strength in the homogeneous limit is not demonstrated.

Similar to the case of CD, the apparent proportionality to the s-sine modulated sum explains why $g_{lum}(\omega)$ is so sensitive to extended couplings. The fact that this proportionality is maintained for disordered MOPV4 is quite remarkable. It indicates that the dependence of $g_{lum}(\omega)$ on extended interactions survives despite the exciton coherence being limited to only 1 or 2 chromophoric units.

Note that the form of eq 10, as derived in ref 26, is the result of a first-order perturbative approach in W/ω_0, which is expected to

break down for MOPV4, where $W = 150$ meV and $\omega_0 = 172$ meV. However, Figure 3 demonstrates that the scaling of $g_{\mathrm{lum}}(\omega)$ with the modulated sum is somehow valid beyond the perturbative regime. This applies to the homogeneous limit, as well as the disordered case. For the latter, we have established 10 analytically using perturbation theory, as will be presented in the following two sections.

3. SINGLE IMPURITY SCATTERING MODEL

Increasing disorder leads to localization of the lowest-energy emitting wave function, to the point where the exciton is substantially localized to only a single chromophore, which has the lowest transition energy of all chromophores in the aggregate. In the single-impurity scattering (SIS) model, this situation is simplified by taking the assumption that all chromophores have the same transition energy $\omega_{0-0} + D$, except for one lower-energy chromophore, which is considered an impurity at site $\overline{n}$ with a corresponding energy of $\omega_{0-0} + D - \Delta$ ($\Delta > 0$). In spite of its simplicity, the SIS model offers a better understanding of the way disorder affects the dependence of $g_{\mathrm{lum}}(\omega)$ on extended interactions, since it allows for an analytic evaluation of eq 10. As it turns out, even when the exciton is almost entirely localized on a single impurity, the g_{lum} line strengths are proportional to a modulated sum over the excitonic interactions.

In this section, the SIS model is utilized to determine the spectral line strengths. In doing so, the bandwidth is assumed to be much smaller than the trap depth Δ of the impurity, thereby allowing for a perturbative expansion in W/Δ. Using the Hamiltonian as defined in eq 2, while setting $\Delta_n = -\delta_{n,\overline{n}}\Delta$ and treating the excitonic coupling as a perturbation, the $\overline{n}$-dependent lowest-energy eigenstate to first order is found to be

$$\begin{aligned}|\Psi^{(\mathrm{em})}(\overline{n})\rangle &= |\overline{n}, \tilde{\nu} = 0\rangle \\ &- \sum_{m\neq\overline{n}}\sum_{\tilde{\nu}'=0,1,\ldots} f_{\tilde{\nu}',0} f_{\tilde{\nu}=0,0}\frac{J_{m,\overline{n}}}{\Delta + \tilde{\nu}'\omega_0}|m,\tilde{\nu}'\rangle \\ &- \sum_{m\neq\overline{n}}\sum_{\tilde{\nu}'=0,1,\ldots}\sum_{\nu''=1,2,\ldots} f_{\tilde{\nu}',0} f_{\tilde{\nu}=0,\nu''}\frac{J_{m,\overline{n}}}{\Delta + (\tilde{\nu}' + \nu'')\omega_0}|m,\tilde{\nu}';\overline{n},\nu''\rangle \\ &+ O[(W/\Delta)^2] \end{aligned} \tag{11}$$

Here the factor $f_{\tilde{\nu},\nu} \equiv \langle\tilde{\nu}|\nu\rangle$ accounts for the overlap between the harmonic oscillator eigenfunctions of $\tilde{\nu}$ vibrational quanta in the shifted potential and ν quanta in the unshifted potential. The first term in eq 11 represents a localized vibronic excitation at the impurity position $\overline{n}$ with $\tilde{\nu} = 0$ vibrational quanta in the shifted excited state potential. The second term consists of one-particle contributions, which corresponds to a delocalization of the polaron's center of mass. In contrast, the third term, constituted of two-particle states, accounts for the radial distribution of the polaron.

The $0-\nu_t$ emission line strength is obtained by inserting the wave function $|\Psi^{(\mathrm{em})}(\overline{n})\rangle$ into eq 5. Averaging over the impurity position $1/N\,\Sigma_{\overline{n}}$, we obtain for all $\nu_t \geq 0$

$$\begin{aligned} I^{0-\nu_t} &= I_{\mathrm{SM}}^{0-\nu_t}\left[1 - 2\Gamma^{0-\nu_t}(\Delta)\frac{1}{N}\sum_{\overline{n},s} J_{\overline{n},\overline{n}+s}\cos(\phi s)\right] \\ &+ O[(W/\Delta)^2] \end{aligned} \tag{12}$$

The second term in the square brackets represents a distortion to the single-molecule emission line strength $I_{\mathrm{SM}}^{0-\nu_t}$. This line strength is determined by Franck–Condon factors, which are the squares of the vibrational overlap factors

$$I_{\mathrm{SM}}^{0-\nu_t} = (f_{\tilde{\nu}=0,\nu_t})^2 = \frac{\exp(-\lambda^2)\lambda^{2\nu_t}}{\nu_t!} \tag{13}$$

The function $\Gamma^{0-\nu_t}(\Delta)$, which we call the "vibrational factor", contains the contributions of exciton-vibrational coupling and the detuning Δ

$$\Gamma^{0-\nu_t}(\Delta) \equiv \sum_{\tilde{\nu}=0,1,\ldots}\frac{f_{\tilde{\nu},0}^2}{\Delta + (\tilde{\nu} + \nu_t)\omega_0} \tag{14}$$

In a similar fashion, by using eq 8, the rotational strength $R_{\mathrm{lum}}^{0-\nu_t}$ is obtained. The resulting g_{lum} line strength then reads

$$\begin{aligned} g_{\mathrm{lum}}^{0-\nu_t} &\equiv \frac{4R_{\mathrm{lum}}^{0-\nu_t}}{I^{0-\nu_t}} \\ &= -2kd\Gamma^{0-\nu_t}(\Delta)\frac{1}{N}\sum_{\overline{n},s} J_{\overline{n},\overline{n}+s}\, s\sin(\phi s) + O[(W/\Delta)^2] \end{aligned} \tag{15}$$

Similar to eq 12, this expression is valid for all $\nu_t \geq 0$. Equation 15 shows that $g_{\mathrm{lum}}(\omega)$ scales as the $s\sin(\phi s)$-modulated sum, independent of the trap depth Δ. This means that the scaling is also entirely independent of the exciton coherence size, which shrinks with increasing delta. The latter follows directly from the exciton coherence function. Following its definition as given in ref 25, this function takes up a very simple form in the SIS model, that is

$$C^{(\mathrm{em})}(s) = \mathrm{e}^{-\lambda^2}\left(\delta_{s,0} - \frac{2}{N}\Gamma^{0-0}(\Delta)\sum_{\overline{n}} J_{\overline{n},\overline{n}+s}\right) + O[(W/\Delta)^2] \tag{16}$$

Increasing Δ causes the coherence function to narrow, resulting in a diminishing coherence range. In the limit of strong disorder (large Δ), the latter approaches zero.

In comparing eqs 12 and 15, we observe that, although g_{lum} scales as an $s\sin(\phi s)$-modulated sum over the couplings, the deviation of PL from the single-molecule value is determined by a $\cos(\phi s)$-modulated sum. These two kinds of modulations to the excitonic interactions are plotted in Figure 4, together with the unmodulated couplings, all taken for the case of MOPV4. This picture clearly presents the much longer range of the s sine-modulation as compared to the cosine-modulation. The inset of Figure 4 demonstrates the sums $(1/N)\Sigma_{n,s}J_{n,n+s}\cos(\phi s)$ and $(1/N)\Sigma_{n,s}J_{n,n+s}s\sin(\phi s)$ for the limit of $N \rightarrow \infty$, as a function of N_{tr}. Whereas the cosine-modulated sum shows a fast convergence, the s sine-modulated sum is characterized by a significant oscillation that extends even beyond $N_{\mathrm{tr}} = 30$. This accounts for the sensitivity of $g_{\mathrm{lum}}(\omega)$ to extended interactions, as opposed to the case of PL.

For finite size aggregates, the contribution of long-range interactions to the modulated sum is suppressed due to the aggregate length. As a result, the modulated sum for an $N = 15$ aggregate deviates from the long-aggregate case. This is illustrated in Figure 5, where the s-sine-modulated sums are displayed for $N = 15$ (solid lines) and $N \rightarrow \infty$ (dashed lines). Also shown are the calculated 0–0 (black circles), 0–1

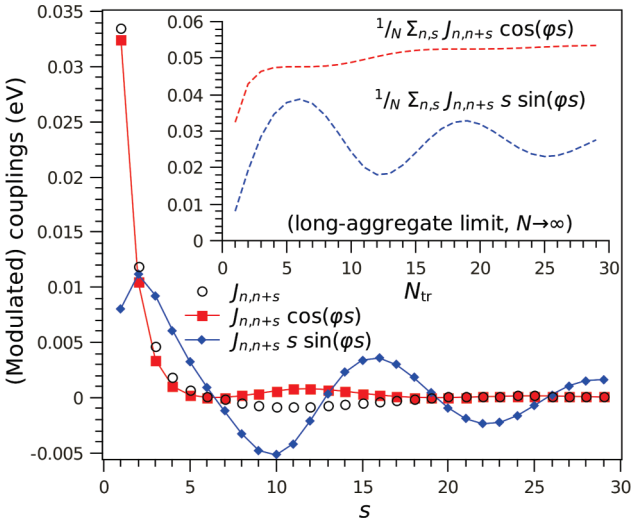

Figure 4. Excitonic interactions for an MOPV4 aggregate (black open circles) as a function of the interchromophoric separation s, taken from ref 25, together with the cos(ϕs)-modulated (red squares) and s sin(ϕs)-modulated (blue diamonds) couplings. Inset shows the sums over these modulated couplings for the long-aggregate limit, as a function of the truncation distance N_{tr}.

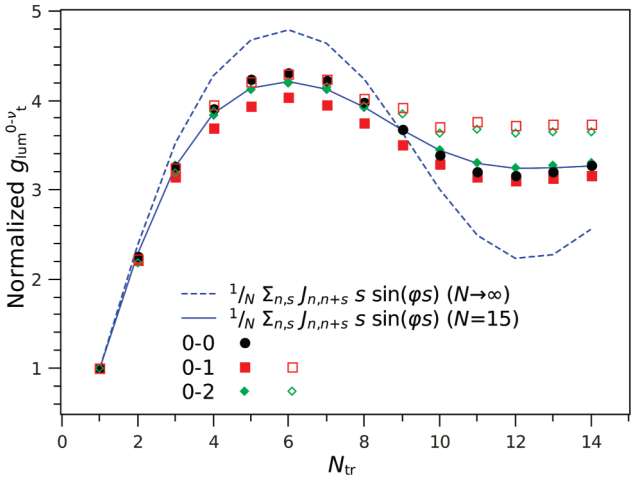

Figure 5. Calculated CPL dissymmetry line strengths as a function of the truncation of the couplings N_{tr}, for the homogeneous limit (open symbols) and including a disorder of σ = 85 meV (closed symbols), together with the s sine-modulated sum over couplings for the infinite-size aggregate (dashed line) and the case of an N = 15 aggregate (solid line). Shown are the line strengths for ν_t = 0 (black circles), 1 (red squares), and 2 (green diamonds), taken from Figure 3, which corresponds to the case of MOPV4. All spectra are divided by the N_{tr} = 1 value.

(red squares), and 0−2 (green diamonds) g_{lum} line strengths, for the homogeneous limit (open symbols) and the disordered case (closed symbols), all taken from Figure 3. The spectra are normalized to the N_{tr} = 1 value. The line strengths nicely follow the modulated sum for the N = 15 aggregate. The fact that better agreement is obtained for a disordered case is in accordance with our findings in Figure 3, where the net g_{lum} line strengths displayed smaller deviations from a constant value for disorder as compared to the homogeneous limit.

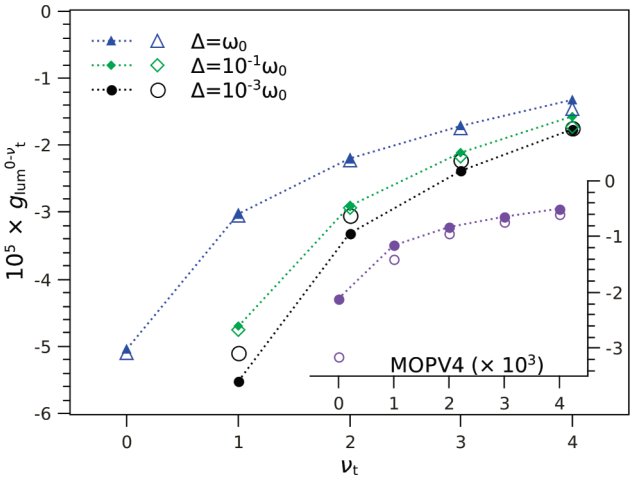

Figure 6. CPL dissymmetry line strengths from the SIS model for a detuning Δ of ω_0 (blue triangles), $10^{-1}\omega_0$ (green diamonds) and $10^{-3}\omega_0$ (black circles). Shown are the numerical results (closed symbols connected by dotted lines) together with the analytical outcome of eq 15 (open symbols). The aggregate under consideration consists of N = 15 chromophores which interact through point-dipole couplings, with a nearest-neighbor coupling of $J_{NN} = 10^{-2}\omega_0$. The maximum number of vibrational quanta ν_{max} is set to 6. All other parameters are the same as in Figure 2. The inset shows the case of MOPV4, with corresponding couplings and a detuning of Δ = 85 meV. Excitonic interactions are not truncated.

The s sine-modulated sum accounts for the ability of CPL dissymmetry to sense extended couplings. Equation 15 illustrates that this sensitivity is preserved in the presence of an impurity. The effect of the detuning parameter Δ is contained entirely in the vibrational factor, which acts as a prefactor to the modulated sum. Apparently, the impurity affects all couplings in a uniform way so that extended interactions maintain their relative contribution to $g_{lum}(\omega)$.

Figure 6 shows a comparison between the analytical outcome of eq 15 (open symbols) and numerical results (closed symbols connected by dotted lines), for different values of the trap depth Δ. The aggregate under consideration consists of N = 15 chromophores. In this case, the different chromophores couple to each other through the well-known point−dipole interactions, for which $J_{n,m} = J_0 \cos[(n - m)\phi]/|n - m|^3$. The nearest-neighbor coupling is set to $J_{NN} = 10^{-2}\omega_0$, where the vibrational energy ω_0 equals 172 meV. Both in the analytical and the numerical cases, the total number of vibrational quanta is limited to ν_{max} = 6, whereas excitonic interactions are not truncated. The other parameters are $\omega_{0-0} + D$ = 2.53 eV, λ^2 = 1.2, and d = 3.75 Å. The numerical simulation is performed by following the method outlined in section 2, while including a single impurity and averaging over the impurity position.

The accuracy of eq 15 is nicely illustrated by Figure 6. The analytical expression, being the result of perturbation theory in W/Δ, is expected to reproduce the numerical results well when the trap depth is large as compared to the bandwidth. Indeed, for Δ as large as ω_0 (blue triangles), the analytical and numerical results are in excellent agreement. Surprisingly, almost perfect agreement is achieved even for a detuning as small as $\Delta = 10^{-2}\omega_0$ (not shown), a value for which $W/\Delta \approx 1$ is beyond the perturbative regime. This agreement is excellent, apart from

dx.doi.org/10.1021/jp2053019 |J. Phys. Chem. B 2011, 115, 10592–10603

the small discrepancy that is observed for increasing ν_t, due to the truncation ν_{max} of the total of vibrational quanta.

A further lowering of Δ causes the SIS model to break down, leading to a significant difference between the analytical and numerical outcome for $\Delta = 10^{-3}\omega_0$ (black circles). For a detuning this small, the excitonic coupling starts to dominate, resulting in the delocalization of the emitting exciton, characteristic of the homogeneous limit. Albeit the SIS model and the homogeneous limit are very different in nature, the corresponding expressions for the g_{lum} line strengths are strikingly similar (compare eq 15 and eq 28 of ref 26). However, there is a subtle, yet essential difference. In the latter case, the s sine-modulated sum is affected by the appearance of pure-excitonic coefficients $\phi_{\bar{k},n}$ of the emitting wave function. In the SIS model, the s sine-modulated sum comes out undisturbed, since the detuning causes the wave function to collapse into a localized state, setting $\phi_{\bar{k},n} \approx \delta_{\bar{n},n}$. On the other hand, for a homogeneous aggregate whose length N exceeds 20, the pure-excitonic wave function coefficients approach a constant value of $1/N$,[26] making the analytical expression of the corresponding sideband g_{lum} line strengths equivalent to eq 15.

In the SIS model, g_{lum}^{0-0} behaves in a similar fashion as the sideband replicas. Figure 6 shows that eq 15 accurately describes the corresponding numerical result for $\Delta = \omega_0$. For smaller values of Δ, the magnitude of the 0−0 line strength shows a dramatic increase (not shown in Figure 6), which is accounted for by the corresponding analytical expression scaling as $1/\Delta$. Still, good agreement between analytical and numerical results is observed for $\Delta = 10^{-1}\omega_0$.

The inset of Figure 6 displays a similar comparison between eq 15 and the full numerical calculations for the case of an MOPV4 aggregate. The latter is mimicked by setting Δ equal to the disorder deviation σ = 85 meV and incorporating the appropriate MOPV4 excitonic interactions. The corresponding free exciton bandwidth, W = 150 meV, is somewhat larger than the trap depth, invalidating perturbation theory. Nevertheless, eq 15 still performs well in reproducing the sideband g_{lum} line strengths. Note that, although the SIS model underestimates the magnitude of the line strengths in the case of point−dipole interactions and small detuning (black circles), for MOPV4 aggregates the magnitudes are overestimated. This difference is due to the larger exciton bandwidth of MOPV4, and the interplay between this bandwidth, the trap depth and the vibronic relaxation energy.

The SIS model accounts for the salient features of $g_{lum}(\omega)$, and its simple form conveniently demonstrates the dependence of $g_{lum}(\omega)$ on extended interactions. At the same time, the model is successful in reproducing the g_{lum} line strengths as compared to numerical results, even for $W \approx \Delta$, where the perturbative approximation is supposed to break down. This makes the SIS model a perfect tool for qualitatively understanding helical MOPV4 aggregates. Nevertheless, the case of smaller disorder is not described adequately by the model of a single impurity. In the next section, a similar perturbative method is utilized to incorporate disorder in its full presence.

4. DISORDER IN THE WEAK COUPLING REGIME

In the weak coupling regime, where the bandwidth W is much smaller than the vibrational energy ω_0, a perturbative approximation in the parameter W/ω_0 is valid. This has been utilized in ref 26 to evaluate the g_{lum} line strengths in the homogeneous limit. The effect of disorder was introduced in the last section, using the example of a single detuned chromophore. The corresponding expression for $g_{lum}(\omega)$, being the result of a perturbative approximation in W/Δ, required the detuning Δ of the impurity to be much greater than the bandwidth. In the current section, we allow every chromophore to be detuned according to the Gaussian distribution introduced in section 2, without posing any limitations on the standard deviation σ. We only require $W \ll \omega_0$, thus performing analysis by employing the weak coupling regime. The current approach is an improvement over the SIS model, since it accounts for the full distribution of disorder. Yet the outcome is very similar to what was obtained in section 3. It will become clear that the effect of disorder on the g_{lum} line strengths is contained entirely in a generalized vibrational factor $\Gamma^{0-\nu_t}(n,n+s)$, which acts as a distortion to the s sine-modulated sum over couplings.

Although the perturbation parameter W/ω_0 naturally suggests the full excitonic coupling to act as a perturbation, we decided to distinguish between single-particle intraband (constant $\tilde{\nu}$) coupling and all other excitonic interactions. The single-particle intraband coupling is included in the unperturbed Hamiltonian, which expressed in terms of one- and two-particle states reads

$$\begin{aligned} H^0 = & \sum_{n,\tilde{\nu}} [\tilde{\nu}\omega_0 + \Delta_n] |n,\tilde{\nu}\rangle\langle n,\tilde{\nu}| \\ & + \sum_{n,\tilde{\nu}} \sum_{n',\nu'} [(\tilde{\nu}+\nu')\omega_0 + \Delta_n] |n,\tilde{\nu};n',\nu'\rangle\langle n,\tilde{\nu};n',\nu'| \\ & + \sum_{n,n'} J_{n,n'} \sum_{\tilde{\nu}} f_{\tilde{\nu},0}^2 |n,\tilde{\nu}\rangle\langle n',\tilde{\nu}| + \omega_{0-0} + D \end{aligned} \tag{17}$$

This Hamiltonian is configuration dependent, as are its eigenstates and eigenenergies. In what follows, the annotation of configuration dependence (C) is dropped for the sake of simplicity. Within the localized basis set, all two-particle states are eigenstates of the unperturbed Hamiltonian. Single-particle states are mixed due to the intraband coupling, so that the single-particle eigenstates to zeroth order are delocalized vibrons

$$|k,\tilde{\nu}\rangle^0 = \sum_n \phi_{k,n}^{(\tilde{\nu})} |n,\tilde{\nu}\rangle \qquad (\tilde{\nu} = 0,1,\ldots) \tag{18}$$

with a corresponding eigenenergy indicated as $E_{k,\tilde{\nu}}^0$. We emphasize that this energy is computed numerically by diagonalization of H^0.

Whereas the single-particle intraband coupling is incorporated in the unperturbed Hamiltonian, the perturbation includes all other excitonic interactions, that is, interband single-particle couplings as well as interactions involving two-particle states. It is expressed as

$$\begin{aligned} H^1 = & \sum_{n,n'} J_{n,n'} \Bigg[\sum_{\tilde{\nu}} \sum_{\tilde{\nu}'\neq\tilde{\nu}} f_{\tilde{\nu},0} f_{\tilde{\nu}',0} |n,\tilde{\nu}\rangle\langle n',\tilde{\nu}'| \\ & + [\sum_{\tilde{\nu},\tilde{\nu}'} \sum_{\nu} f_{\tilde{\nu},\nu} f_{\tilde{\nu}',0} |n,\tilde{\nu}\rangle\langle n',\tilde{\nu}';n,\nu| + \text{h.c.}] \\ & + \sum_{\tilde{\nu},\tilde{\nu}'} f_{\tilde{\nu},0} f_{\tilde{\nu}',0} \sum_{m,\nu} |n,\tilde{\nu};m,\nu\rangle\langle n',\tilde{\nu}';m,\nu| \\ & + \sum_{\tilde{\nu},\tilde{\nu}'} \sum_{\nu,\nu'} f_{\tilde{\nu},\nu} f_{\tilde{\nu}',\nu'} |n,\tilde{\nu};n',\nu'\rangle\langle n',\tilde{\nu}';n,\nu| \Bigg] \end{aligned} \tag{19}$$

The configuration-dependent emitting state to first order consists of the lowest-energy single-particle eigenstate $|\bar{k},\tilde{\nu}=0\rangle^0$ plus first-order corrections due to the perturbation H^1, that is

$$|\Psi^{(\mathrm{em})}\rangle = |\bar{k},\tilde{\nu}=0\rangle^0 + \sum_k \sum_{\tilde{\nu}'\geq 1} \sum_{n,m} \frac{J_{n,m}\phi_{k,n}^{(\tilde{\nu}')}\phi_{\bar{k},m}^{(\tilde{\nu}=0)} f_{\tilde{\nu}',0} f_{\tilde{\nu}=0,0}}{E^0_{k,\tilde{\nu}=0} - E^0_{k,\tilde{\nu}'}} |k,\tilde{\nu}'\rangle^0 + \sum_{n,\tilde{\nu}'} \sum_{n',\nu'} \frac{J_{n,n'}\phi_{\bar{k},n'}^{(\tilde{\nu}=0)} f_{\tilde{\nu}',0} f_{\tilde{\nu}=0,\nu'}}{E^0_{\bar{k},\tilde{\nu}=0} - E_{n,\tilde{\nu}';n',\nu'}} |n,\tilde{\nu}';n',\nu'\rangle \quad (20)$$

where the two-particle energy is given by $E_{n,\tilde{\nu}';n',\nu'} = \omega_{0-0} + D + (\tilde{\nu}'+\nu')\omega_0 + \Delta_n$. Note that the k value that minimizes the zeroth-order eigenenergy is indicated as $\bar{k}$. Similar to the SIS model, the second term in eq 20 accounts for the delocalization of the polaron's center of mass, whereas the third term describes the extent of the polaron radius.

Substituting the resulting emitting state into eq 8 leads to the g_{lum} line strength. For the sideband region, the result is

$$g_{\mathrm{lum}}^{0-\nu_t} = -2kd \sum_{n,s} \Gamma^{0-\nu_t}(n,n+s) J_{n,n+s} s \sin(\phi s) + O[(W/\omega_0)^2] \quad (21)$$

This expression is strikingly similar to eq 15. However, the vibrational factor now appears inside the modulated sums. Being n- and s-dependent, this "generalized vibrational factor" contains both the effects of exciton-vibrational coupling and disorder

$$\Gamma^{0-\nu_t}(n,n+s) \equiv \phi_{\bar{k},n}^{(\tilde{\nu}=0)^2} \sum_{\tilde{\nu}'} \frac{f^2_{\tilde{\nu}',0}}{E_{n+s,\tilde{\nu}';n,\nu_t} - E^0_{\bar{k},\tilde{\nu}=0}} \quad (22)$$

Since all configurational dependence is contained in the generalized vibrational factor, performing an average over disorder configurations leaves the general form of $g_{\mathrm{lum}}^{0-\nu_t}$ intact but solely involves the replacement

$$\Gamma^{0-\nu_t}(n,n+s) \rightarrow \langle \Gamma^{0-\nu_t}(n,n+s)(C)\rangle_C$$

As it turns out, the SIS model is actually a special case of the model introduced in this section. When the distributed disorder is reduced to a single impurity with corresponding trap depth Δ, the emitting wave function collapses into a state localized at the impurity position $\bar{n}$, while the wave function coefficient is reduced to $\phi_{k,n}^{(\tilde{\nu}=0)} = \delta_{n,\bar{n}} + O[W/\Delta]$. The corresponding energy is $E^0_{\bar{k},\tilde{0}} = \omega_{0-0} + D - \Delta + O[W/\Delta]$. To first order in W/Δ, this localized state couples to two-particle states $|\bar{n}+s,\tilde{\nu};\bar{n},\nu_t\rangle$ $(s>0)$ with energies $E_{\bar{n}+s,\tilde{\nu};\bar{n},\nu_t} = \omega_{0-0} + D + (\tilde{\nu}+\nu_t)\omega_0$. Hence, the generalized vibrational factor in eq 22 loses its n- and s-dependence. Taking an average over the impurity position then directly leads to the $g_{\mathrm{lum}}^{0-\nu_t}$ expression for the SIS model.

The homogeneous limit follows in an analogous way. Since in this limit all energies become n- and s-independent, all of the generalized vibrational factor can be factored out of the modulated sum, except for the wave function coefficients. What comes out is the expression derived earlier in ref 26.

Using eq 21, the sideband g_{lum} line strengths are calculated semianalytically. After a numerical diagonalization of the unperturbed Hamiltonian as defined in eq 17, the resulting zeroth-order wave function coefficients and eigenenergies are substituted in eq 22. Figure 7 shows the outcome (open symbols) together with full-numerical results, obtained by utilizing the method described in section 2 (closed symbols). Similarly to what was done in section 2, distributed disorder is modeled by randomly drawing the transition energy offsets from a normal distribution, using a width of σ = 8.5 meV. In order to fulfill the weak-coupling limit ($W \ll \omega_0$), point-dipole interactions are used (black symbols) with a corresponding nearest-neighbor coupling of $J_{\mathrm{NN}} = 10^{-2}\omega_0$, where ω_0 = 172 meV. Also shown in Figure 7 are the results for MOPV4 interactions (violet symbols), with a corresponding disorder width of σ = 85 meV. In both cases the couplings are not truncated, and the results are averaged over a total of 10^5 disorder configurations. The other parameters are N = 15, $\omega_{0-0} + D$ = 2.53 eV, λ^2 = 1.2, $\nu_{\max}$ = 4, and d = 3.75 Å. Excitonic interactions are not truncated.

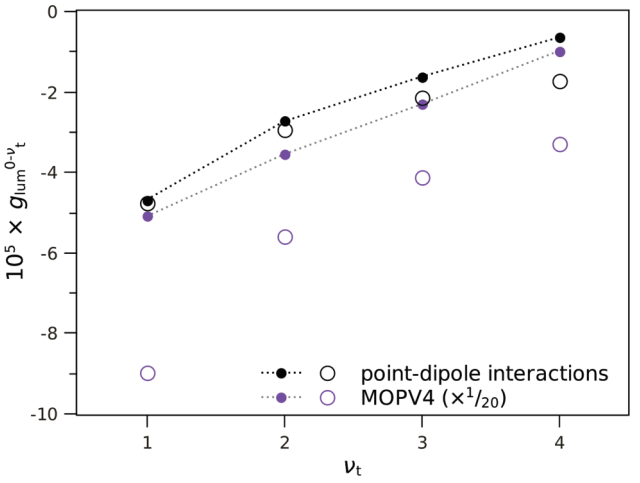

Figure 7. CPL dissymmetry line strengths calculated both semianalytically using eq 21 (open symbols) and fully numerically using the method outlined in section 2 (closed symbols connected by dotted lines). Shown are the results incorporating untruncated point-dipole interactions with a nearest-neighbor coupling of $J_{\mathrm{NN}} = 10^{-2}\omega_0$ (black) and using MOPV4 interactions (violet), with disorder widths of σ = 8.5 and 85 meV, respectively. In the latter case, the line strengths are divided by a factor of 20. All other parameters are the same as in Figure 2.

For the case of point-dipole interactions, Figure 7 demonstrates good agreement between the numerical results and the semianalytical outcome following eq 21, confirming the validity of this expression in the weak-coupling limit. Especially g_{lum}^{0-1} is reproduced almost perfectly. The deviations that occur for $\nu_t \geq 3$ are due to truncation of the total number of vibrational quanta beyond $\nu_{\max}$. Obviously, in the intermediate coupling regime ($W \approx \omega_0$), the perturbative approximation in the parameter W/ω_0 breaks down, giving less accurate results for MOPV4. As shown in Figure 7, the semianalytical outcome overestimates the g_{lum}^{0-1} line strength by about 75% in this case.

In the weak coupling limit the generalized vibrational factor acts as a distortion to the modulated sum, thereby affecting the dependence of the g_{lum} line strengths on excitonic interactions. Nevertheless, as long as $\Gamma^{0-\nu_t}(n,n+s)$ shows nearly constant behavior for different values of $(n,n+s)$, $g_{\mathrm{lum}}^{0-\nu_t}$ is still approximately proportional to the s-sine-modulated sum. It is therefore possible to extract valuable information on the g_{lum} line strengths by analyzing the generalized vibrational factor. This has been carried out for the case of point-dipole interactions, as discussed

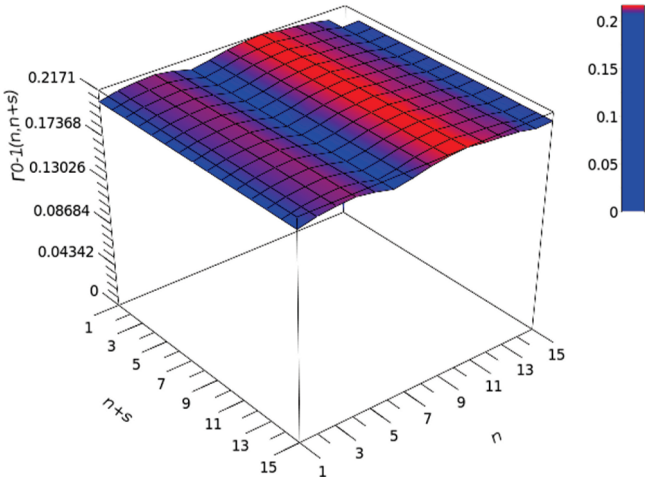

Figure 8. Calculated profile of the generalized vibrational factor for $\nu_t = 1$, obtained by numerically evaluating eq 22. Untruncated point-dipole interactions are used, with a corresponding nearest-neighbor coupling of $J_{NN} = 10^{-2}\omega_0$. An average over 10^5 disorder configurations is taken, using a disorder width of $\sigma = 8.5$ meV. All other parameters are the same as in Figure 2.

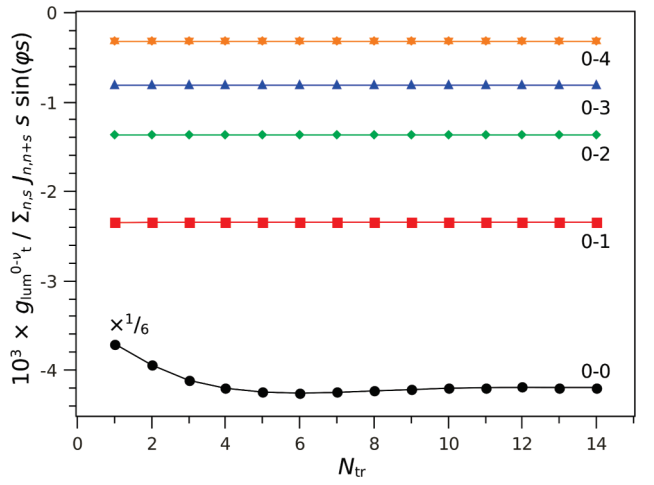

Figure 9. Calculated CPL dissymmetry line strengths divided by the s-sin(ϕs)-modulated sum over excitonic interactions as a function of the truncation of the couplings, for $\nu_t = 0$ (black circles), 1 (red squares), 2 (green diamonds), 3 (blue triangles), and 4 (orange stars). Point-dipole interactions are used, with a nearest-neighbor coupling of $J_{NN} = 10^{-2}\omega_0$. The disorder width is $\sigma = 8.5$ meV. All other parameters are the same as in Figure 2. The results for the 0−0 line strengths are rescaled by a factor of 1/6.

earlier in Figure 7. The generalized vibrational factor is calculated numerically and averaged over a total of 10^5 disorder configurations, with $\sigma = 8.5$ meV. Figure 8 shows the result for the 0−1 transition.

It is clearly demonstrated in Figure 8 that $\Gamma^{0-1}(n,n+s)$ deviates only slightly from a constant value throughout the entire $(n,n+s)$ interval. A profile is weakly manifested along the n-coordinate. This profile is the result of energetic randomness and disappears upon increasing the number of configurations. Overall, $\Gamma^{0-1}(n,n+s)$ is constant within 2.5%. Similar results have been obtained for the vibrational factors corresponding to the lower-energy sidebands ($\nu_t \geq 2$). In all cases, the vibrational factor demonstrates a divergence for $s = 0$ which does not interfere with $g_{lum}(\omega)$ since the $s = 0$ contribution does not count in the s sin(ϕs)-modulated sum. In Figure 8, $\Gamma^{0-1}(n,n)$ is set manually to the minimum of $\Gamma^{0-1}(n,n' \neq n)$ for the ease of demonstration.

Being approximately constant, the vibrational factor can be factored out of the modulated sum in eq 21, resulting in an undisturbed scaling of the sideband g_{lum} line strengths with the s sine-modulated sum. As a consequence, the corresponding net g_{lum} line strengths, obtained after dividing the line strengths by the s sine-modulated sum, are expected to be perfectly flat for different values of N_{tr}. Figure 9 shows that this is indeed the case. Further analysis of $\Gamma^{0-\nu_t}(n,n+s)$ reveals that its constant behavior is of statistical nature. Its value strongly fluctuates among different individual disorder configurations, yet the averaging over the total ensemble makes $\Gamma^{0-\nu_t}(n,n+s)$ to converge to a value which is practically independent of n and s. Increasing the number of disorder configurations from 10^5 to 10^6 causes the vibrational factors to level off even further.

Also shown in Figure 9 are the net g_{lum}^{0-0} line strengths. In contrast to the sideband, the CPL dissymmetry in the $\nu_t = 0$ region is not described by eq 21. Nevertheless, according to Figure 9, the 0−0 line strength approximately scales with the s-sine-modulated sum. In accordance with our earlier findings, this result is valid provided that the disorder is strong enough to strongly localize the exciton.

5. CONCLUSIONS AND DISCUSSION

CPL dissymmetry is a powerful technique for probing extended excitonic interactions in helical molecular assemblies. Its ability to sense distant interactions derives from the scaling of $g_{lum}(\omega)$ with a sum over excitonic couplings modulated by the distance s times the sine of ϕs, where ϕ is the pitch angle. This sensitivity occurs in the well-studied MOPV4 helices, where truncating the interactions beyond the sixth nearest-neighbor results in a 30% increase in the magnitude of $g_{lum}(\omega)$, despite an imperceptible change in the unpolarized photoluminescence spectrum.[25]

In ref 26, the proportionality of $g_{lum}(\omega)$ to the modulated sum (in the sideband region of the spectrum) was established in the absence of disorder, or the "homogeneous limit". In our current work, we have shown that this proportionality is more robust and even survives the presence of strong disorder, where excitons are essentially localized on a single chromophore.

In the weak-coupling limit, where the free excitonic bandwidth W is much smaller than the vibrational energy ω_0, the perturbation analysis of section 4 yields a simple expression for the CPL dissymmetry corresponding to the sideband transitions, which clearly reflects the linear dependence of g_{lum} on the modulated sum. This dependence remains valid even into the intermediate coupling regime, appropriate for MOPV4, as is demonstrated numerically in Figure 3. In the case of strong coupling, the g_{lum} spectrum eventually levels off, becoming independent of the interactions, as shown in an earlier study.[27]

The dependence of $g_{lum}(\omega)$ on extended interactions in the presence of strong disorder is quite surprising, since the disorder causes the coherence range of the emitting exciton to approach zero. The mechanism behind this dependence is best explained by considering a single detuned chromophore (impurity) in an otherwise homogeneous chain, the so-called SIS model, see section 3. As indicated by eq 15, all interactions are affected uniformly by the presence of the impurity, thereby preserving the relative contribution of each interaction $J_{n,n+s}$.

It was previously shown that a similar dependence on extended interactions is characteristic of the CD signal.[12−18] References 17 and 18 demonstrated that the first moment of the CD spectrum scales linearly as the s sine-modulated sum over the couplings, independent of the magnitude of disorder as well as the strength of the vibronic coupling. An analogous result for the first moment of $g_{lum}(\omega)$ does not hold, for reasons explained in section 2.

As indicated in Figure 3, the 0−0 g_{lum} line strength scales approximately as the s $\sin(\phi s)$-modulated sum in the disordered case, although it demonstrates a more pronounced deviation than the sideband line strengths. In the SIS model, the 0−0 line strength scales in the same way as the sideband dissymmetries, as eq 15 holds for all $\nu_t \geq 0$. Decreasing the disorder parameter Δ/W results in a relative surge in the magnitude of g_{lum}^{0-0} as compared to the sideband dissymmetries. The enhancement reflects the increasing exciton coherence length.[26]

The sensitivity of CPL dissymmetry to extended interactions translates to a dependence of $g_{lum}(\omega)$ on the aggregate length N, since for small aggregates the contributions of long-range interactions to the g_{lum} spectrum are suppressed, as is emphasized in section 3. The dependence on N can be utilized to experimentally extract the spatial form of extended interactions for molecular systems in which the aggregate length can be controlled accurately. In doing so, no details about the energetic disorder and exciton-vibrational coupling are required, since these factors do not affect the scaling of $g_{lum}(\omega)$ with the modulated sum over couplings. This puts $g_{lum}(\omega)$ next to CD as a valuable tool for probing the electronic structure of helical aggregates.

AUTHOR INFORMATION

Corresponding Author

*E-mail: spano@temple.edu.

ACKNOWLEDGMENT

R.T. was supported by the Dutch Ministry of Education, Culture and Science through a grant in the Huygens Scholarship Programme. A.S. acknowledges The Netherlands Organization for Scientific Research for support through a VENI grant. F.C.S. is supported by the NSF, Grant No. DMR 0906464.

REFERENCES

(1) Rodger, A.; Norden, B. *Circular Dichroism and Linear Dichroism*; Oxford University Press: Oxford, 1997.

(2) Nakanishi, K., Berova, N., Woody, R. W., Eds.; *Circular Dichroism Principles and Applications*; Wiley-VCH: New York, 2000.

(3) Gonzalez-Rodriguez, A.; Schenning, A. P. H. J. *Chem. Mater.* **2011**, *23*, 310.

(4) Hoeben, F. J. M.; Jonkheijm, P.; Meijer, E. W.; Schenning, A. P. H. J. *Chem. Rev.* **2005**, *105*, 1491.

(5) Schenning, A. P. H. J.; Meijer, E. W. *Chem. Commun.* **2005**, 3245.

(6) Eisele, D. M.; Knoester, J.; Kirstein, S.; Rabe, J. P.; Vanden Bout, D. A. *Nat. Nanotechnol.* **2009**, *4*, 658.

(7) Stradomska, A.; Knoester, J. *J. Chem. Phys.* **2010**, *133*, 094701.

(8) Vlaming, S. M.; Augulis, R.; Stuart, M. C. A.; Knoester, J.; van Loosdrecht, P. H. M. *J. Phys. Chem. B* **2009**, *113*, 2273.

(9) Wu, J. S.; Grimsdale, A. C.; Mullen, K. *J. Mater. Chem.* **2005**, *15*, 41.

(10) Würthner, F. *Chem. Commun.* **2004**, 1564.

(11) Würthner, F.; Chen, Z. J.; Hoeben, F. J. M.; Osswald, P.; You, C. C.; Jonkheijm, P.; von Herrikhuyzen, J.; Schenning, A. P. H. J.; van der Schoot, P.; Meijer, E. W.; Beckers, E. H. A.; Meskers, S. C. J.; Janssen, R. A. J. *J. Am. Chem. Soc.* **2004**, *126*, 10611.

(12) Harada, N.; Chen, S. L.; Nakanishi, K. *J. Am. Chem. Soc.* **1975**, *97*, 5345.

(13) Matile, S.; Berova, N.; Nakanishi, K.; Fleischhauer, J.; Woody, R. W. *J. Am. Chem. Soc.* **1996**, *118*, 5198.

(14) Lewis, F. D.; Liu, X. Y.; Wum, Y. S.; Zuo, X. B. *J. Am. Chem. Soc.* **2003**, *125*, 12729.

(15) Tsubaki, K.; Takaishi, K.; Tanaka, H.; Miura, M.; Kawabata, T. *Org. Lett.* **2006**, *8*, 2587.

(16) Somsen, O. J. G.; van Grondelle, R.; van Amerongen, H. *Biophys. J.* **1996**, *71*, 1934.

(17) Burin, A. L.; Armbruster, M. E.; Hariharan, M.; Lewis, F. D. *Proc. Natl. Acad. Sci. U.S.A.* **2009**, *106*, 989.

(18) van Dijk, L.; Bobbert, P. A.; Spano, F. C. *J. Phys. Chem. B.* **2010**, *114*, 817.

(19) Langeveld-Voss, B. M. W.; Janssen, R. A. J.; Meijer, E. W. *J. Mol. Struct.* **2000**, *521*, 285.

(20) Lakhwani, G.; Koeckelberghs, G.; Meskers, S. C. J.; Janssen, R. A. J. *Chem. Phys. Lett.* **2007**, *437*, 193.

(21) Langeveld-Voss, B. M. W.; Beljonne, D.; Shuai, Z.; Janssen, R. A. J.; Meskers, S. C. J.; Meijer, E. W.; Bredas, J. L. *Adv. Mater.* **1998**, *10*, 1343.

(22) Meskers, S. C. J.; Peeters, E.; Langeveld-Voss, B. M. W.; Janssen, R. A. J. *Adv. Mater.* **2000**, *12*, 589.

(23) Kawagoe, Y.; Fujiki, M.; Nakano, Y. *New J. Chem.* **2010**, *34*, 637.

(24) Nakano, Y.; Liu, Y.; Fujiki, M. *Polym. Chem.* **2010**, *1*, 460.

(25) Spano, F. C.; Meskers, S. C. J.; Hennebicq, E.; Beljonne, D. *J. Am. Chem. Soc.* **2007**, *129*, 7044. *J. Am. Chem. Soc.* **2007**, *129*, 16278.

(26) Spano, F. C.; Meskers, S. C. J.; Hennebicq, E.; Beljonne, D. *J. Chem. Phys.* **2008**, *129*, 024704.

(27) Spano, F. C.; Zhao, Z.; Meskers, S. C. J. *J. Chem. Phys.* **2004**, *120*, 10594.

(28) Schenning, A. P. H. J.; Jonkheijm, P.; Peeters, E.; Meijer, E. W. *J. Am. Chem. Phys.* **2001**, *123*, 409.

(29) Jonkheijm, P.; van der Schoot, P.; Schenning, A. P. H. J.; Meijer, E. W. *Science* **2006**, *313*, 80.

(30) Herz, L. M.; Daniel, C.; Silva, C.; Hoeben, F. J. M.; Schenning, A. P. H. J.; Meijer, E. W.; Friend, R. H.; Phillips, R. T. *Phys. Rev. B* **2003**, *68*, 045203.

(31) Beljonne, D.; Hennebicq, E.; Daniel, C.; Hertz, L. M.; Silva, C.; Scholes, G. D.; Hoeben, F. J. M.; Jonkheim, P.; Schenning, A. P. H. J.; Meijer, E. W. *J. Phys. Chem. B* **2005**, *109*, 10594.

(32) Prins, P.; Senthilkumar, K.; Grozema, F. C.; Jonkheijm, P.; Schenning, A. P. H. J.; Meijer, E. W.; Siebbeles, L. D. A. *J. Phys. Chem. B* **2005**, *109*, 18267.

(33) Daniel, C.; Westenhoff, S.; Makereel, F.; Friend, R. H.; Beljonne, D.; Herz, L. M.; Silva, C. *J. Phys. Chem. C* **2007**, *111*, 19111.

(34) van Dijk, L.; Kersten, S. P.; Jonkheijm, P.; van der Schoot, P.; Bobbert, P. A. *J. Phys. Chem. B* **2008**, *112*, 12386.

(35) Cornil, J.; Beljonne, D.; Heller, C. M.; Campbell, I. H.; Laurich, B. K.; Smith, D. L.; Bradley, D. D. C.; Mullen, K.; Bredas, J. L. *Chem. Phys. Lett.* **1997**, *278*, 139.

(36) Holstein, T. *Ann. Phys.* **1959**, *8*, 325.

(37) Spano, F. C. *J. Chem. Phys.* **2002**, *116*, 5877.

(38) Philpott, M. R. *J. Chem. Phys.* **1971**, *55*, 2039.

(39) The cubic frequency dependence of the PL spectum is omitted, in order to focus on the line strengths. For $g_{lum}(\omega)$, this cubic frequency dependence cancels out automatically.

(40) Mayo, S. L.; Olafson, B. D.; Goddard, W. A. *J. Phys. Chem.* **1990**, *94*, 8897.

(41) Note that in ref 25 a value for σ that was used is $(2)^{1/2}$ times the σ = 85 meV used in our current work. This stems from σ being defined differently in ref 25.

(42) The 0−0 transition for ϕ = 0 is strictly symmetry forbidden in aggregates with even values of N. For N = 15, as used in this work, the 0−0 transition is vanishingly small.

(43) In ref 26, an unusual sign change between g_{lum}^{0-0} and the sidebands was shown to exist in disorder-free helices between $n + 1/2$ and $n + 1$ complete turns. However, this result is specific for even values of N. In the current case with $N = 15$, the sign change occurs only for the truncation value of $N_{tr} = 2$, as shown in Figure 2a. For all other truncation values, there is no relative sign change.

(44) Harada, N.; Nakanishi, K. *Circular Dichroic Spectroscopy*; University Science Books: Mill Valley CA, 1983.

(45) Didraga, C.; Klugkist, J. A.; Knoester, J. *J. Chem. Phys. B* **2002**, *106*, 11474.

(46) Didraga, C.; Knoester, J. *J. Phys. Chem.* **2004**, *121*, 10687.